

Cavity-Heisenberg spin- j chain quantum battery and reinforcement learning optimization

Peng-Yu Sun, Hang Zhou, and Fu-Quan Dou*

College of Physics and Electronic Engineering, Northwest Normal University, Lanzhou, 730070, China

Machine learning offers a promising methodology to tackle complex challenges in quantum physics. In the realm of quantum batteries (QBs), model construction and performance optimization are central tasks. Here, we propose a cavity-Heisenberg spin chain quantum battery (QB) model with spin- j ($j = 1/2, 1, 3/2$) and investigate the charging performance under both closed and open quantum cases, considering spin-spin interactions, ambient temperature, and cavity dissipation. It is shown that the charging energy and power of QB are significantly improved with the spin size. By employing a reinforcement learning algorithm to modulate the cavity-battery coupling, we further optimize the QB performance, enabling the stored energy to approach, even exceed its upper bound in the absence of spin-spin interaction. We analyze the optimization mechanism and find an intrinsic relationship between cavity-spin entanglement and charging performance: increased entanglement enhances the charging energy in closed systems, whereas the opposite effect occurs in open systems. Our results provide a possible scheme for design and optimization of QBs.

I. INTRODUCTION

Quantum mechanics has attracted considerable attention due to its importance in driving scientific and technological progress, ranging from quantum communication [1, 2], quantum sensing [3, 4], to quantum computing [5, 6]. Among these, quantum thermodynamics has emerged as a field that aims to reconstruct thermodynamics through the fundamental laws of quantum mechanics, and one of its important tasks is to focus on work, heat, and entropy within a quantum framework [7–9]. In the realm of energy storage, the concept of the quantum battery (QB) has been proposed by applying the principles of quantum thermodynamics to revolutionize conventional battery technology [10–12]. Experiments have also shown advances towards the exploration of quantum batteries (QBs) [13–18].

Model construction of a QB is prerequisite for its realization. With various QB models proposed [19–27], two theoretical models have gained traction: cavity QBs [28–37] and spin chain QBs [38–56]. Cavity QBs rely on the properties of quantum cavities or optical resonators to store and release energy by controlling the interaction between the cavity and the battery which provides advantages in rapid charging [32–34]. Spin chain QBs utilize quantum entanglement to enhance the efficiency and speed of energy storage. Large spin QBs further employ collective spin states in ensembles of magnetic ions or molecules, which provide high-energy storage [57, 58]. A significant development is the cavity-Heisenberg spin chain QB, which combines the benefits of a spin chain and quantum cavities. The integration enhances stored energy, increases charging power, and demonstrates a quantum advantage [59]. Besides, open QBs consider factors such as dissipation and decoherence, and can be used to address issues related to stable charging and energy loss

[29, 56, 60–67].

Performance optimization is also a crucial topic in QB research. Current optimization methods include the utilization of quantum resources [24, 30, 37, 44, 54, 62, 68, 69], control of charging modes [27, 39–41, 70–76], using of model characteristics [35, 45–50, 77, 78], and consideration non-Markovian dynamics [36, 64, 66, 79–81]. However, precise control over complex systems often presents challenges for practical application. Fortunately, the rapid development of reinforcement learning (RL) has shown promising applications in the quantum domain [82–90]. Especially in QBs, RL has been applied to optimise the charging process in Dicke QBs, which leads to higher energy extraction and greater charging precision compared to conventional methods [91]. It has also been used to develop stable charging protocols for micromaser QBs, which significantly enhances their overall efficiency [92]. In RL algorithms, the soft actor-critic (SAC) algorithm offers a more advanced solution that enables efficient and adaptive optimization of complex parameter spaces. This approach not only accelerates the exploration of possible configurations but yields more precise and reliable performance improvements [93, 94].

Inspired by the development of QBs, we focus on two main issues. One is how to construct a more efficient QB model by combining cavity QBs with large spin QBs. The other is whether the performance of this QB can be further optimized through RL. In this work, we propose a cavity-Heisenberg spin chain QB model with large spins, where the stored energy, charging power, and entanglement property of the QBs for the chain with spin- $1/2$, spin- 1 , and spin- $3/2$ configuration are explored. The charging performance of the QBs can be effectively modulated by means of spin size, cavity-spin coupling and spin-spin interactions. Furthermore, we study the cavity QBs in the case of open systems with ambient temperature and cavity dissipation. Based on the SAC algorithm, the charging process in both closed and open systems are optimized through tuning the cavity-spin coupling pa-

* doufq@nwnu.edu.cn

parameter, where an intrinsic relationship between cavity-spin entanglement and charging performance is revealed that the increased entanglement enhances charging energy in a closed system, whereas the opposite effect occurs in the open system.

The rest of paper is organized as follows. In Sec. II we introduce the cavity-Heisenberg large-spin chain QB, performance metrics, and the RL optimization algorithm. In Sec. III the charging process of the QB with three different spin configurations in a closed system are investigated, where the influence of entanglement and the RL optimization on the cavity QB are studied. Furthermore, we examine the charging dynamics of the QB in an open system and explore the corresponding entanglement properties and the RL optimization in Sec. IV. Finally, a brief conclusion is given in Sec. V.

II. MODEL AND APPROACH

We consider a cavity-Heisenberg large-spin chain QB model, which consists of single-mode cavity as the charger and a Heisenberg spin chain with spin-spin interactions as the battery, as shown in the QB part of Fig. 1. The whole system can be described by the Hamiltonian

$$H = H_C + H_B + \lambda(t)H_I, \quad (1)$$

where H_C and H_B represent the charger and the battery, and H_I is the interaction term with the charging time interval $\lambda(t)$ given by a step function equal to 1 for $t \in [0, T]$ and zero elsewhere. The various terms (hereafter we set $\hbar = 1$) can be expressed as

$$H_C = \omega_c \hat{a}^\dagger \hat{a}, \quad (2)$$

$$H_B = \omega_a \sum_{n=1}^N \hat{S}_n^z + \omega_a J \sum_{n=1}^{N-1} [(1 + \gamma) \hat{S}_n^x \hat{S}_{n+1}^x + (1 - \gamma) \hat{S}_n^y \hat{S}_{n+1}^y + \Delta \hat{S}_n^z \hat{S}_{n+1}^z], \quad (3)$$

$$H_I = g \sum_{n=1}^N (\hat{S}_n^+ + \hat{S}_n^-) (\hat{a}^\dagger + \hat{a}), \quad (4)$$

where \hat{a} (\hat{a}^\dagger) is annihilation (creation) operator and the cavity field frequency is ω_c . \hat{S}_n^i with $i = x, y, z$ are the spin operators of the site n and J is the nearest-neighbor interaction between spins. ω_a is the frequency of spins and the strength of the spin-cavity coupling is given by the parameter g . γ and Δ are the anisotropy coefficients and N is the number of spins. \hat{S}_n^+ (\hat{S}_n^-) represents the raising (lowering) operator. In the case of spin-1/2 particles, \hat{S}_n^i is the spin Pauli operators on site n . In order to ensure the maximum energy transfer, we will focus on the resonance regime (*i.e.*, $\omega_a = \omega_c = 1$), and the off-resonance case $\omega_a \neq \omega_c$ will not be considered since it

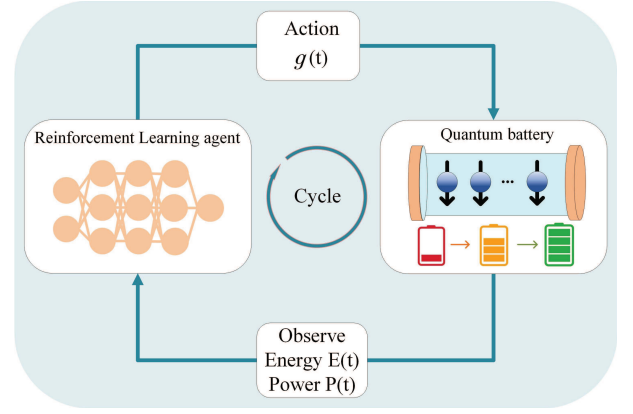


FIG. 1. Schematic diagram of an RL algorithm for optimising the charging performance of a cavity-Heisenberg spin chain QB. An RL agent determines the external control action of the cavity-spin coupling $g(t)$ by observing the current state of stored energy $E(t)$ and average charging power $P(t)$ of the QB, thereby maximizing the power under the maximizing stored energy. The optimization process consists of numerous iterations between the RL algorithm and the QB. Through this cycle, QB charging efficiency is refined to its optimal level.

characterizes a less efficient energy transfer between the cavity and spins. In all calculations, for simplicity, we take the parameters $N = 3$, $\gamma = 0.4$, and $\Delta = 1$. Numerical work has been performed by using PyTorch [95] and QuTiP2 toolbox [96].

At time $t \leq 0$, the QB is prepared in the ground state of H_B and coupled to a single-mode cavity in the N photons' Fock-state. Thus, the initial state of the total system is

$$|\psi(0)\rangle = |G\rangle_B \otimes |N\rangle_C. \quad (5)$$

When environmental factors are taken into account, the system is treated as open, and the dynamic process of the QB charging can be described by solving the Lindblad master equation

$$\frac{d\rho(t)}{dt} = -\frac{i}{\hbar} [H, \rho(t)] + \mathfrak{D}[\rho(t)], \quad (6)$$

where $\rho(t)$ is the density matrix of the system at time t . $\mathfrak{D}[\cdot]$ represents the dissipative superoperator. In the open system, the QB has a practical significance only when the cavity dissipation κ is much greater than spin dissipative κ_s , *i.e.*, $\kappa \gg \kappa_s$. We only consider the effects of dissipation and ambient temperature on the cavity field, and ignore the interaction between spin and environment. Therefore, the dissipative superoperator $\mathfrak{D}[\cdot]$ can be expressed as

$$\mathfrak{D}[\rho(t)] = \frac{1}{2} \kappa (n_{th} + 1) [2a\rho(t)a^\dagger - a^\dagger\rho(t)a - \rho(t)a^\dagger a] + \frac{1}{2} \kappa n_{th} [2a^\dagger\rho(t)a - aa^\dagger\rho(t) - \rho(t)aa^\dagger], \quad (7)$$

where $n_{th} = 1/\{\exp[(\hbar\omega_c)/(k_B T)] - 1\}$ is the mean occupation number of the boson heat bath. k_B is the Boltzmann constant and T is the ambient temperature. When $\kappa = 0$, the environment has no influence on the system and the system is a closed one.

The stored energy $E(t)$ and the average charging power $P(t)$ are two typical metrics for charging performance of QB, which can be defined as

$$E(t) = \text{Tr}[H_B \rho_B(t)] - \text{Tr}[H_B \rho_B(0)], \quad (8)$$

$$P(t) = E(t)/t, \quad (9)$$

where $\rho_B(t)$ is the reduced density matrix of the QB at the time t . The entanglement between the cavity and the spin can be given by the logarithmic negativity [59, 97]

$$E_{\mathcal{N}} = \log_2 \|\rho^{T_B}\|_1, \quad (10)$$

where the ρ^{T_B} denotes the partial matrix of ρ with respect to the subsystem B .

The SAC algorithm is one of outstanding RL algorithms and has already been applied in the field of quantum physics such as seeking improved control policies in quantum thermal machines [98]. We will employ the SAC algorithm to optimize the charging performance of the QB. As shown in Fig. 1, the optimization process is illustrated, where the RL agent is a neural network to optimize the cavity QB by tuning the interaction between charger and battery. The RL agent manages an external control function $g(t)$, which influences the cavity-battery coupling and its action is based on the current status of charging performance by observing $E(t)$ and $P(t)$. The observed results of the two functions are further fed back to the RL agent who would adjust the control parameter $g(t)$ in order to maximize the stored energy $E(t)$ and average charging power $P(t)$. The optimization procedure can be realized by a continuous cyclic process exploring the state-action space and refining policy, so that the charging efficiency of QBs can be continuously improved to the optimal level. The details of the SAC algorithm are presented in Appendix A.

III. CLOSED SYSTEM: $\kappa = 0$

We first study the charging properties of the QB in the case of closed system which corresponds to the dissipative parameter $\kappa = 0$. To investigate the behavior of the QB during the charging process, we calculate the time-dependent of stored energy $E(t)$, average charging power $P(t)$, and the entanglement $E_{\mathcal{N}}(t)$ between the cavity and the spin chain with different spin- j configurations, and the results are illustrated in Fig. 2 for the cavity-spin coupling $g = 1$. It shows that the larger the spin- j of QB, the greater the energy $E(t)$, the power $P(t)$ as well as the entanglement $E_{\mathcal{N}}(t)$ between charger and battery. In the charging procedure, the stored energy

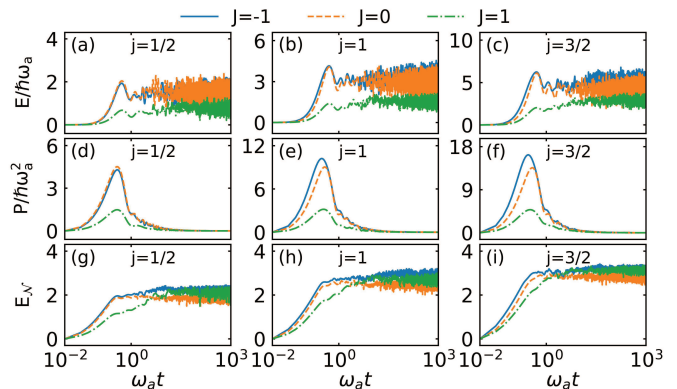


FIG. 2. The dependence of (a)-(c) the stored energy $E(t)$ (in units of $\hbar\omega_a$), (d)-(f) average charging power $P(t)$ (in units of $\hbar\omega_a^2$), and (g)-(i) logarithmic negativity $E_{\mathcal{N}}(t)$ of closed system QB as a function of $\omega_a t$ for different values of spin j . The different curves in these plots stand for various spin-spin interaction J , as indicated in the legends. The cavity-spin coupling is chosen as $g = 1$.

$E(t)$ and the cavity-spin entanglement $E_{\mathcal{N}}(t)$ have the similar behaviors. This is because that the energy occupancy of QB changes from the lowest energy state to some higher energy states (see Appendix B for details), which results in the entanglement increasing correspondingly in the evolution of closed system. Moreover, the performance of QBs are also influenced by the spin-spin interaction, where the antiferromagnetic interaction ($J > 0$) may diminish charging efficiency.

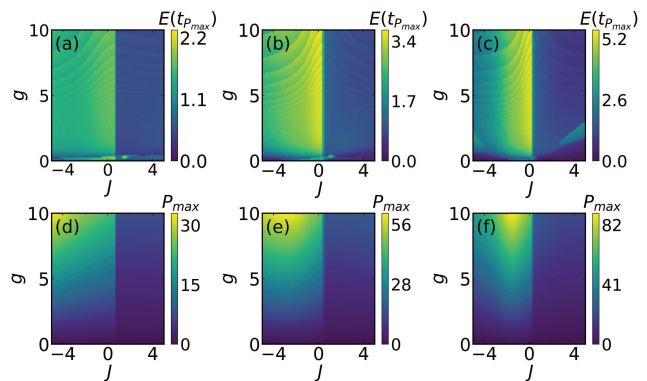


FIG. 3. The contour plots of closed system QB's (a)-(c) stored energy $E(t_{P_{max}})$ (in units of $\hbar\omega_a$), and (d)-(f) maximum charging power P_{max} (in units of $\hbar\omega_a^2$) as functions of the cavity-spin coupling strength g and spin-spin interaction strength J for different spin j : (a) and (d) spin-1/2, (b) and (e) spin-1, (c) and (f) spin-3/2.

It is noted that the stored energy $E(t)$ of the QBs exhibits an oscillation phenomenon, which presents a challenge to achieving the maximal storage energy. A potential solution is to cease the charging process when the average charging power $P(t)$ of the QB reaches its peak, and the energy and its corresponding power at this

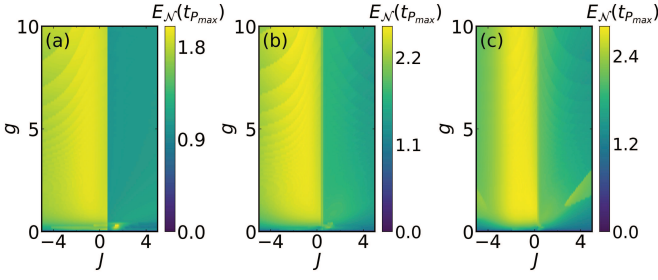


FIG. 4. The logarithmic negativity $E_{\mathcal{N}}(t_{P_{max}})$ as functions of the cavity-spin coupling strength g and spin-spin interaction strength J for different spin j : (a) spin-1/2, (b) spin-1, and (c) spin-3/2.

specific moment can be labeled as $E(t_{P_{max}})$ and P_{max} respectively. We analyze the influence of the cavity-spin coupling g and the spin-spin interaction strength J on the $E(t_{P_{max}})$ and P_{max} for different spin- j configurations. The energy and the corresponding charging power as the functions of the parameters g and J are shown in Fig. 3. It is shown that the cavity-spin coupling and the spin-spin interaction can modulate effectively the energy $E(t_{P_{max}})$ and the power P_{max} , and the QB with higher spin configuration can achieve better charging performance. In addition, the strong antiferromagnetic spin-spin interaction results in the lower $E(t_{P_{max}})$ and P_{max} , and the enhanced cavity-spin coupling g can boost the charging power P_{max} . The high stored energy range occurs in regions where the interaction is weak. When antiferromagnetic interaction approaches a critical value, the charging efficiency suddenly becomes low, i.e., both the stored energy and the charging power become smaller. Along with the increase of the spin size, on the one hand the energy $E(t_{P_{max}})$ and the power P_{max} will increase, and on the other hand the zone of the maximum of average charging power P_{max} will move in the parameter space of J and g (yellow regions in the second row of Fig. 3). This means that for a small spin system, a large ferromagnetic spin-spin interaction is necessary to achieve a high charging power, and for a large spin QB, only a weak ferromagnetic spin-spin interaction is required to obtain a high charging power.

In order to analyze the above property of the maximal stored energy, it is necessary to investigate the entanglement between the charger and the battery since the stored energy and the cavity-spin entanglement exhibits the similar dynamical behaviours in Fig. 2. Figure 4 illustrates the cavity-spin entanglement $E_{\mathcal{N}}(t_{P_{max}})$ at maximal average power for different spin- j configurations, where the entanglements are functions of cavity-spin coupling g and spin-spin interaction J . It is obvious that the entanglement $E_{\mathcal{N}}(t_{P_{max}})$ in Fig. 4 have the consistent behaviors in comparison with those of maximal stored energy $E(t_{P_{max}})$ in Fig. 3, where the maximal cavity-spin entanglement can be obtained without resorting to the strong spin-spin interaction along with the increasing of spin size. This indicates a positive correlation between

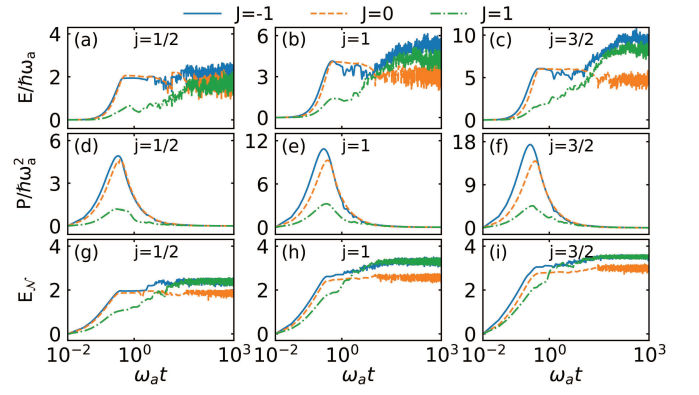


FIG. 5. Optimized results: (a)-(c) The dependence of the stored energy $E(t)$ (in units of $\hbar\omega_a$), (d)-(f) average charging power $P(t)$ (in units of $\hbar\omega_a^2$), and (g)-(i) logarithmic negativity $E_{\mathcal{N}}(t)$ of closed system QB as a function of $\omega_a t$ for different spin j .

the cavity-spin entanglement and the QB performance in closed QB system. The maximal storage energy $E(t_{P_{max}})$ can be adjusted by tuning the cavity-spin entanglement $E_{\mathcal{N}}(t_{P_{max}})$.

The SAC algorithm represents an exemplary approach to machine learning, exhibiting remarkable capabilities in addressing complex tasks. Here, we employ this algorithm to optimize the performance of the QB by adjusting the cavity-spin coupling $g(t)$. In order to facilitate a comparison with the results obtained prior to optimisation, the coupling range is selected to be within the interval $[0, 1]$. The RL agent learns to maximize the $E(t)$ and then ensure the maximum $P(t)$. The $E(t)$ and $P(t)$ of the QB serve as the observed state input of the agent, which enables the agent to modulate the coupling strength between the cavity and the battery as the action output of the QB. Through continuous iteration, the pathway of cavity spin coupling is continuously updated and optimized. As a result, the performance of QB is enhanced.

The optimized results of the stored energy $E(t)$, average charging power $P(t)$, and the corresponding entanglement $E_{\mathcal{N}}(t)$ between the cavity and spin for different spin- j configurations are presented in Fig. 5. In comparison with the performance of the pre-optimization QB in Fig. 2, we find that no matter which spin configurations, the QB's stored energy can be improved following the optimized process, and can approach, even exceed its upper bound without spin-spin interaction. Here the upper bounds of the stored energy are $2jN\hbar\omega_a$ for spin- j , respectively. Similarly, large spin corresponds to higher energy. Over time, the stored energy is divided into two stages: the gradual rise stage (consistent with the case without optimization), and the hold or lift stage. In the stage, the stored energy is maintained or increased after reaching the pre-optimisation maximum. The system without spin-spin interactions belong to the former, while the systems with spin-spin interactions correspond to the latter. More interestingly, different from the previous

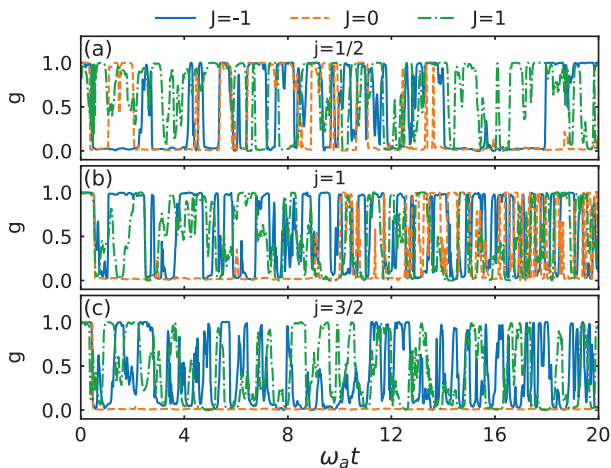


FIG. 6. The optimization pathways of the cavity-spin coupling g for (a) $j = 1/2$, (b) $j = 1$, and (c) $j = 3/2$.

results without optimization, the final stored energy of both ferromagnetic and antiferromagnetic interactions is significantly increased, which is several times higher than that before optimization. We further demonstrate that the SAC algorithm is actually regulating the entanglement between the charger and the battery by adjusting the coupling between the cavity and the battery. In the closed QB system, the coupling between the cavity and the battery is constantly adjusted to increase the entanglement between the charger and the battery. During this process, the energy population distribution corresponding to the QB gradual transitions from the initial occupation of the lowest energy state to the higher energy state. As a result, the QB's stored energy is further increased. The optimization pathways of the cavity-spin coupling g for different QB configurations are illustrated in Fig. 6, which presents only the time period till the stored energy reaches its stable maximum value.

IV. OPEN SYSTEM: $\kappa \neq 0$

In this section, we investigate the charging properties of the QB in the case of open system which introduces ambient temperature and cavity field dissipation.

Figure 7 shows the time-dependent behaviour of the stored energy $E(t)$, average charging power $P(t)$, and the cavity-spin entanglement $E_{\mathcal{N}}(t)$ for QBs with different ambient temperatures and cavity field dissipations. In the open QB system, all QBs can achieve stable charging due to the environmental factors cancelling out the oscillation effect. Here, this energy transfer is purely quantum-mechanical effects, which are generated by the collective behaviour of the battery, charger, and surrounding environment [99]. However, the final stable energy behaves differently for different spin configurations. For a spin-1/2 QB, the final stable energy is less than the maximum value, whereas for a spin-1 and spin-

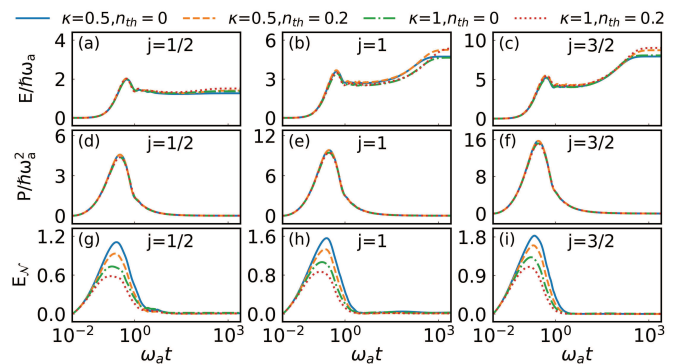


FIG. 7. The dependence of (a)-(c) the stored energy $E(t)$ (in units of $\hbar\omega_a$), and (d)-(f) average charging power $P(t)$ (in units of $\hbar\omega_a^2$), and (g)-(i) logarithmic negativity $E_{\mathcal{N}}(t)$ of open system QB as a function of $\omega_a t$ for different spin j . The different curves stand for various ambient temperature and cavity dissipation. The parameters are chosen as $g = 1$, $J = -1$.

3/2 QB, the final stable energy is higher than the maximum value. Similarly, larger spins correspond to larger maximum stored energy and maximum average charging power, while the cavity-battery entanglement decreases over time in the open systems. During the earlier stage of the charging process, the cavity-spin interaction induces an increase in the entanglement between the charger and the battery, accompanied by a transition in the energy population of the QB from the lowest to higher energy states. In the middle stage, the charging energy $E(t)$ and the cavity-spin entanglement $E_{\mathcal{N}}(t)$ exhibit different behaviors where the charging energy maintains stability but the entanglement drops rapidly and tends to zero. This is due to the fact that, although the energy population of QB remains essentially unchanged, the entanglement $E_{\mathcal{N}}(t)$ between the charger and the battery is transferred to the environment as a result of the open system evolution. In the final stage of the charging process, the cavity-spin entanglement maintains a value close to zero since it is transferred to the environment almost completely, but the energy occupancy of QB tends to much higher energy states, resulting in a further rise of the charging energy $E(t)$ (see also Appendix B).

To analyze the effect of ambient temperature and cavity dissipation on the charging energy and the physical mechanism of charging process, we calculate the stable stored energy (here defined as $E(\infty)$) and the cavity-battery entanglement (defined as $E_{\mathcal{N}}(\infty)$) as a function of them, and these results are shown in Fig. 8 and Fig. 9 for different spin and spin-spin interactions. For all spin configurations QB, the final stable stored energy increases as the ambient temperature increases. Interestingly, the effect of cavity dissipation differs for different spin-spin interactions. In the ferromagnetic interaction, the strong dissipation shows a positive effect, and the large dissipation leads to the higher stored energy, while in the antiferromagnetic interaction, the dissipation sup-

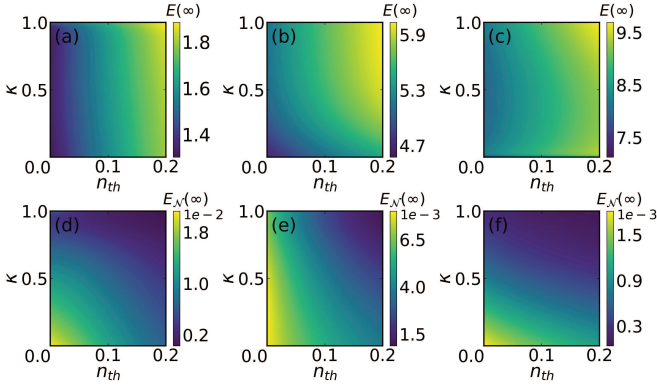


FIG. 8. The contour plots of open system QB's (a)-(c) stable stored energy $E(\infty)$ (in units of $\hbar\omega_a$), and (d)-(f) logarithmic negativity $E_{\mathcal{N}}(\infty)$ as functions of n_{th} and κ with the spin-spin interaction $J = -1$.

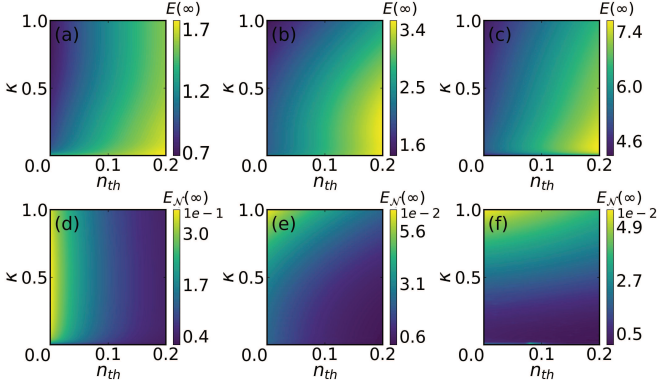


FIG. 9. The contour plots of open system QB's (a)-(c) stable stored energy $E(\infty)$ (in units of $\hbar\omega_a$), and (d)-(f) logarithmic negativity $E_{\mathcal{N}}(\infty)$ as functions of n_{th} and κ with the spin-spin interaction $J = 1$.

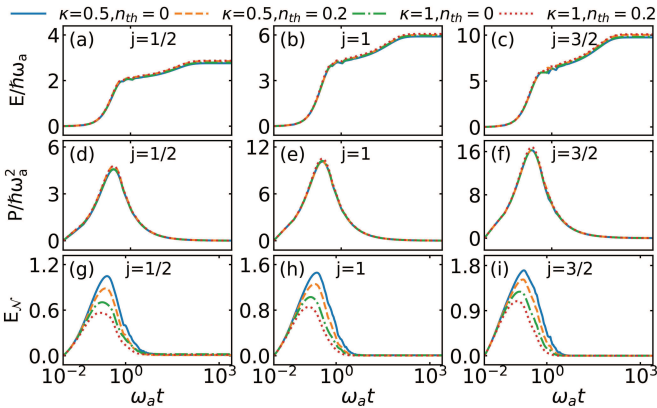


FIG. 10. Optimized Results: (a)-(c) The dependence of the stored energy $E(t)$ (in units of $\hbar\omega_a$), (d)-(f) average charging power $P(t)$ (in units of $\hbar\omega_a^2$), and (g)-(i) logarithmic negativity $E_{\mathcal{N}}(t)$ of open system QB as a function of $\omega_a t$ for different spin j . The parameter is chosen as $J = -1$.

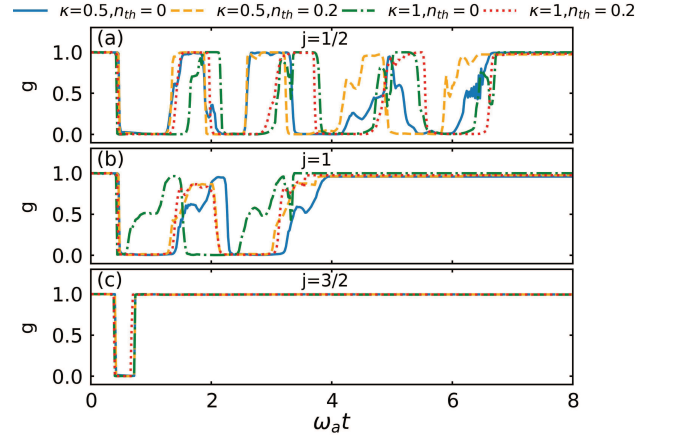


FIG. 11. Pathways under different ambient temperatures and cavity dissipation conditions for (a) $j = 1/2$, (b) $j = 1$, (c) $j = 3/2$.

presses the stable stored energy. Regardless of the spin-spin interactions and spin configurations, the final cavity-charger entanglement shows the opposite behavior to the stable stored energy, with small entanglement leading to large stable stored energy.

We further employ the SAC algorithm to optimize the QB performance by adjusting the cavity-spin coupling g which ranges in $[0, 1]$. The optimized stored energy $E(t)$, average charging power $P(t)$, and corresponding cavity-spin entanglement $E_{\mathcal{N}}(t)$ are presented in Fig. 10. Since the QB performance can be improved regardless of the spin-spin interaction, here we show the ferromagnetic interaction and take $J = -1$. Obviously, the optimized stored energy and the average charging power have increased, and even the stored energy can reach the upper bound of the charging process without spin-spin interaction. Figure 11 illustrates the optimization pathways of the cavity-spin coupling g for different QB configurations (We take $\omega_a t = 8$, and then the coupling stays the same value). The actual optimization process begins when stored energy reaches its maximum before optimization, at which point the cavity-battery coupling is turned off, i.e., $g = 0$. In this way, the environment and the cavity interact, and then the coupling continues, and the cavity acts as a charger to continue to provide energy to the battery, and the battery's stored energy continues to increase due to energy occupancy of QB in higher energy level. This process is repeated until the energy reaches its maximum value. For large spins, such as spin $2/3$, the process is even simpler, and the coupling only needs to be adjusted once to achieve the purpose. Likewise, the stable stored energy corresponds to the minimum cavity-battery entanglement.

V. CONCLUSIONS

We have proposed a cavity-Heisenberg spin chain QB model with spin- j ($j = 1/2, 1, 2/3$) configurations and investigated the charging performance. We have shown that the stored energy and average charging power can be significantly improved with larger spin sizes. The ferromagnetic spin interaction can improve the QB performance, while the anti-ferromagnetic interaction leads to a decrease in the QB's stored energy and average charging power. Additionally, by adjusting the cavity-spin coupling and spin-spin interaction, the QB can achieve higher energy and average charging power. Further, we have considered the effects of the ambient temperature and cavity field dissipation. The open QB can achieve stable charging process and its performance is affected by ambient temperature, cavity dissipation and spin-spin interaction. For the QB with ferromagnetic interaction, the ambient temperature and cavity dissipation have positive effects on the stable stored energy, while for anti-ferromagnetic interaction QB, cavity dissipation will inhibit the stable energy. We have also employed the SAC algorithm in both closed and open systems to optimize the QB performance by adjusting the cavity-spin coupling. The optimization reduces the influence of the various parameters to achieve better QB performance, and its final stored energy can approach, even exceed the upper bound without spin-spin interaction for all spin configurations. We have found that the physical mechanism of optimization process. The charger-battery entanglement can be tuned by adjusting the cavity-battery coupling parameters. In the optimization process of the closed QB system, the cavity-spin entanglement is positively correlated with the stored energy. In contrast, in open QB, the stable stored energy reaches a maximum corresponding to low entanglement. Our result provides new insights for the construction and optimization of future QBs.

ACKNOWLEDGMENTS

We thank Dr. P. A. Erdman for helpful discussions. The work is supported by the National Natural Science Foundation of China (Grants No. 12475026 and No. 12075193).

Appendix A: Principles of the Soft Actor-Critic Algorithm

The SAC algorithm is an RL method designed for continuous action spaces [93, 94]. Its objective is to maximize both the expected reward and the policy entropy. The inclusion of policy entropy promotes randomness in the policy, which enhances exploration and prevents the algorithm from settling into suboptimal solutions. The

objective function of SAC is given by

$$J(\pi) = \sum_t \mathbb{E}_{(s_t, a_t) \sim \rho_\pi} [r(s_t, a_t) + \alpha \mathcal{H}(\pi(\cdot|s_t))],$$

where $J(\pi)$ is the objective of the policy π ; s_t is the state at time t and a_t is the action taken at state s_t ; ρ_π is the state-action distribution induced by policy π , which represents the probability distribution of states and actions under the current policy; $r(s_t, a_t)$ is the reward obtained by taking action a_t in state s_t ; α is the entropy coefficient that controls the trade-off between the accumulated reward and the policy entropy. $\mathcal{H}(\pi(\cdot|s_t))$ is the entropy of the policy π at state s_t , measuring the randomness of the policy. The expectation $\mathbb{E}_{(s_t, a_t) \sim \rho_\pi}$ denotes the weighted average over state-action pairs sampled from the state-action distribution ρ_π .

SAC estimates the value of state-action pairs using the soft Q-function $Q(s_t, a_t)$, which is updated using the Bellman equation

$$Q(s_t, a_t) = r(s_t, a_t) + \gamma \mathbb{E}_{s_{t+1} \sim p} [V(s_{t+1})],$$

where the soft Q-value $Q(s_t, a_t)$ represents the expected cumulative reward after taking action a_t at state s_t , and γ is the discount factor that determines the importance of future rewards. The next state s_{t+1} is reached by taking action a_t in state s_t , with $p(s_{t+1}|s_t, a_t)$ denoting the state transition probability. $V(s_{t+1})$ is the state value function at the next state, computed through the target Q-network. The expectation $\mathbb{E}_{s_{t+1} \sim p}$ is the average over all possible next states, weighted by the state transition probabilities $p(s_{t+1}|s_t, a_t)$.

The policy update is aimed at maximizing both the Q-value and policy entropy. The policy optimization objective is

$$J_\pi = \mathbb{E}_{s_t \sim D} [\mathbb{E}_{a_t \sim \pi} [\alpha \log(\pi(a_t|s_t)) - Q(s_t, a_t)]],$$

here J_π is the policy optimization objective, D is the experience replay buffer, and $\pi(a_t|s_t)$ is the action probability distribution of the policy at state s_t . $\log(\pi(a_t|s_t))$ represents the log probability of action a_t , which contribute to the entropy of the policy. The expectation $\mathbb{E}_{s_t \sim D}$ is the average over samples drawn from the replay buffer D , and $\mathbb{E}_{a_t \sim \pi}$ is the average over the action distribution π for each state s_t , which ensures the policy maximizes the expected Q-value and entropy.

To balance exploration and exploitation, SAC allows for the adaptive tuning of the entropy coefficient α . The goal is to maintain the policy entropy close to a target value $\overline{\mathcal{H}}$. The adjustment objective for α is given by

$$J(\alpha) = \mathbb{E}_{a_t \sim \pi_t} [-\alpha \log(\pi_t(a_t|s_t)) - \alpha \overline{\mathcal{H}}],$$

where $\overline{\mathcal{H}}$ is the target entropy and π_t represents the current policy network. The expectation $\mathbb{E}_{a_t \sim \pi_t}$ is the average over the action probabilities $\pi_t(a_t|s_t)$ under the current policy π_t .

To enhance learning stability, SAC employs soft updates for the target Q-network parameters, which are updated according to the following rule

$$\phi_{\text{target}} \leftarrow \tau \phi + (1 - \tau) \phi_{\text{target}},$$

where ϕ is the current Q-network parameters, ϕ_{target} is the target Q-network parameters, and τ is the soft update coefficient, typically set to a small value to ensure smooth updates.

The SAC algorithm can be summarized in the following steps:

- a. Initialize the policy network π_θ , the double Q-networks Q_{ϕ_1} and Q_{ϕ_2} , and the target Q-network parameters ϕ_{target_1} and ϕ_{target_2} .
- b. Store interaction data in the replay buffer D :
 - Observe the state s_t and take an action a_t .
 - Receive a reward r_t and transition to the next state s_{t+1} .
 - Store (s_t, a_t, r_t, s_{t+1}) in D .
- c. Randomly sample a batch of data from the replay buffer D .
- d. Update the Q-function using the double Q-networks:
 - Compute the target Q-value: $y = r + \gamma \min(Q_{\phi_1}(s_{t+1}, \pi_\theta(s_{t+1})), Q_{\phi_2}(s_{t+1}, \pi_\theta(s_{t+1})))$
 - Update the Q-network parameters ϕ_1 and ϕ_2 by minimizing the mean squared error.
- e. Update the policy network:
 - Update the policy network parameters θ by maximizing the expected Q-value and policy entropy.
- f. Adjust the entropy coefficient α to make the policy entropy close to the target value.
- g. Perform soft updates of the target Q-network parameters:
 - Update the target Q-network parameters using the soft update formula.
- h. Repeat steps b to h until convergence or the maximum number of iterations is reached.

Through these steps, the SAC algorithm is capable of achieving efficient exploration and stable policy learning in complex continuous action spaces, thereby optimizing the energy storage and charging power of the QB.

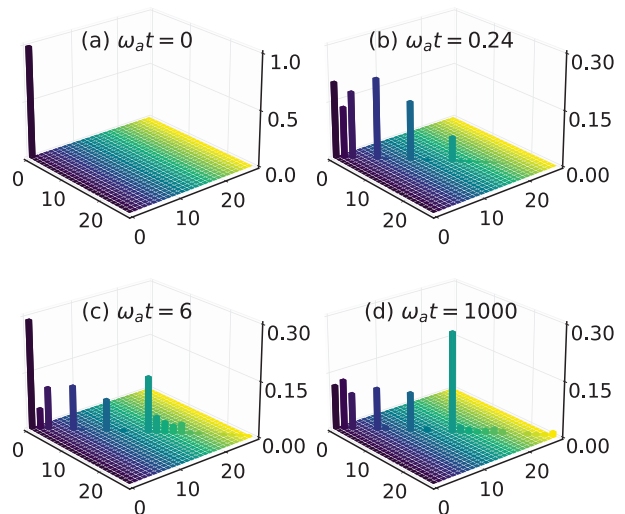


FIG. 12. Projection of $\rho_B(t)$ in the eigenenergy representation of H_B for closed system at different times: (a) $\omega_a t = 0$, (b) $\omega_a t = 0.24$, (c) $\omega_a t = 6$, and (d) $\omega_a t = 1000$. The parameter is chosen as $J = -1$.

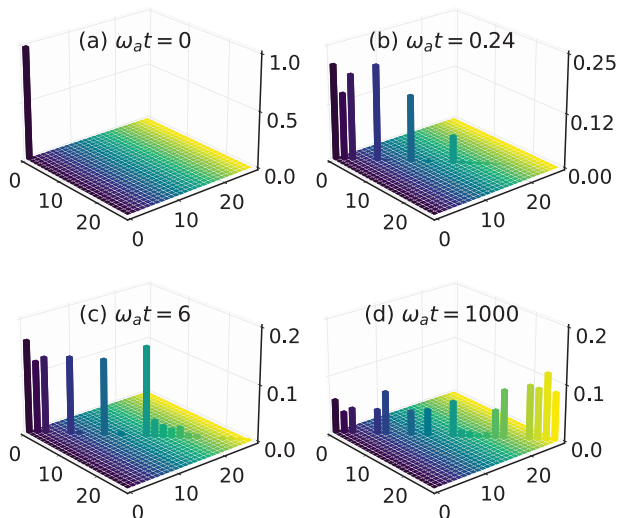


FIG. 13. Projection of $\rho_B(t)$ in the eigenenergy representation of H_B for open system at different times: (a) $\omega_a t = 0$, (b) $\omega_a t = 0.24$, (c) $\omega_a t = 6$, and (d) $\omega_a t = 1000$. The parameters are chosen as $J = -1, \kappa = 0.5, n_{th} = 0.2$.

Appendix B: The energy distribution of QB in Charging Process for Closed and Open Systems

In this appendix, we calculate the projection of the $\rho_B(t)$ in the eigenenergy representation of the H_B at different times, which represents the population in each energy eigenstate. The energy levels of H_B are organized in ascending order, beginning with the lowest energy state and extending to increasingly higher energy states. These

results display in Figs. 12-13 for closed and open system, respectively. For simplicity, we only show the case with spin-1 before optimization. The horizontal axes represent the eigenstate orders of H_B , with the diagonal elements referring to the energy levels of the system, and the vertical axis indicates the occupation probability of each energy eigenstate.

At the initial time in the closed system, the system is in the lowest energy state with no population in higher energy states. As time progresses, the system transfers

population from the lowest energy state to higher energy eigenstates, leading to an increase in energy. In contrast to the closed system, in the open system, at the final stage of the charging process, the energy tends to occupy much higher energy levels, which results in a further rise in the charging energy. Further calculations showed that the similar behaviour emerges in the optimized case, where the population exhibits a more pronounced distribution across higher energy levels, contributing to the increase in charging energy.

-
- [1] C. Nayak, S. H. Simon, A. Stern, M. Freedman, and S. Das Sarma, *Rev. Mod. Phys.* **80**, 1083 (2008).
- [2] J. Eisert and D. Gross, *Phys. Rev. Lett.* **102**, 240501 (2009).
- [3] J. T. Reilly, J. D. Wilson, S. B. Jäger, C. Wilson, and M. J. Holland, *Phys. Rev. Lett.* **131**, 150802 (2023).
- [4] C. L. Degen, F. Reinhard, and P. Cappellaro, *Rev. Mod. Phys.* **89**, 035002 (2017).
- [5] I. Pogorelov, T. Feldker, C. D. Marciniak, L. Postler, G. Jacob, O. Kriegelsteiner, V. Podlesnic, M. Meth, V. Negnevitsky, M. Stadler, B. Höfer, C. Wächter, K. Lakhmanskii, R. Blatt, P. Schindler, and T. Monz, *PRX Quantum* **2**, 020343 (2021).
- [6] P. Kok, W. J. Munro, K. Nemoto, T. C. Ralph, J. P. Dowling, and G. J. Milburn, *Rev. Mod. Phys.* **79**, 135 (2007).
- [7] G. T. Landi and M. Paternostro, *Rev. Mod. Phys.* **93**, 035008 (2021).
- [8] P. Talkner and P. Hänggi, *Rev. Mod. Phys.* **92**, 041002 (2020).
- [9] P. Skrzypczyk, A. J. Short, and S. Popescu, *Nat. Commun.* **5**, 4185 (2014).
- [10] F. Campaioli, F. A. Pollock, and S. Vinjanampathy, “Quantum batteries,” in *Thermodynamics in the Quantum Regime: Fundamental Aspects and New Directions* (2018) pp. 207–225.
- [11] R. Alicki and M. Fannes, *Phys. Rev. E* **87**, 042123 (2013).
- [12] F. Campaioli, S. Gherardini, J. Q. Quach, M. Polini, and G. M. Andolina, *Rev. Mod. Phys.* **96**, 031001 (2024).
- [13] C.-K. Hu, J. Qiu, P. J. P. Souza, J. Yuan, Y. Zhou, L. Zhang, J. Chu, X. Pan, L. Hu, J. Li, Y. Xu, Y. Zhong, S. Liu, F. Yan, D. Tan, R. Bachelard, C. J. Villas-Boas, A. C. Santos, and D. Yu, *Quantum Sci. Technol.* **7**, 045018 (2022).
- [14] J. Q. Quach, K. E. McGhee, L. Ganzer, D. M. Rouse, B. W. Lovett, E. M. Gauger, J. Keeling, G. Cerullo, D. G. Lidzey, and T. Virgili, *Sci. Adv.* **8**, eabk3160 (2022).
- [15] R.-H. Zheng, W. Ning, Z.-B. Yang, Y. Xia, and S.-B. Zheng, *New J. Phys.* **24**, 063031 (2022).
- [16] G. Gemme, M. Grossi, D. Ferraro, S. Vallecorsa, and M. Sasseti, *Batteries* **8**, 43 (2022).
- [17] I. Maillette de Buy Wenniger, S. E. Thomas, M. Maffei, S. C. Wein, M. Pont, N. Belabas, S. Prasad, A. Harouri, A. Lemaître, I. Sagnes, N. Somaschi, A. Auffèves, and P. Senellart, *Phys. Rev. Lett.* **131**, 260401 (2023).
- [18] J. Joshi and T. S. Mahesh, *Phys. Rev. A* **106**, 042601 (2022).
- [19] W.-X. Guo, F.-M. Yang, and F.-Q. Dou, *Phys. Rev. A* **109**, 032201 (2024).
- [20] F. Caravelli, G. Coulter-De Wit, L. P. García-Pintos, and A. Hamma, *Phys. Rev. Res.* **2**, 023095 (2020).
- [21] A. Rojo-Francàs, F. Isaule, A. C. Santos, B. Juliá-Díaz, and N. T. Zinner, *Phys. Rev. A* **110**, 032205 (2024).
- [22] Z. Beleño, M. F. Santos, and F. Barra, *New J. Phys.* **26**, 073049 (2024).
- [23] G. M. Andolina, D. Farina, A. Mari, V. Pellegrini, V. Giovannetti, and M. Polini, *Phys. Rev. B* **98**, 205423 (2018).
- [24] D.-L. Yang, F.-M. Yang, and F.-Q. Dou, *Phys. Rev. B* **109**, 235432 (2024).
- [25] D. Rossini, G. M. Andolina, D. Rosa, M. Carrega, and M. Polini, *Phys. Rev. Lett.* **125**, 236402 (2020).
- [26] A. C. Santos, B. Cakmak, S. Campbell, and N. T. Zinner, *Phys. Rev. E* **100**, 032107 (2019).
- [27] F. Q. Dou, Y. J. Wang, and J. A. Sun, *Europhys. Lett.* **131**, 43001 (2020).
- [28] F. Pirmoradian and K. Mølmer, *Phys. Rev. A* **100**, 043833 (2019).
- [29] Y. Yao and X. Q. Shao, *Phys. Rev. E* **104**, 044116 (2021).
- [30] L. Fusco, M. Paternostro, and G. De Chiara, *Phys. Rev. E* **94**, 052122 (2016).
- [31] G. M. Andolina, M. Keck, A. Mari, M. Campisi, V. Giovannetti, and M. Polini, *Phys. Rev. Lett.* **122**, 047702 (2019).
- [32] D. Ferraro, M. Campisi, G. M. Andolina, V. Pellegrini, and M. Polini, *Phys. Rev. Lett.* **120**, 117702 (2018).
- [33] X. Zhang and M. Blaauuboer, *Front. Phys.* **10**, 1097564 (2023).
- [34] A. Crescente, M. Carrega, M. Sasseti, and D. Ferraro, *Phys. Rev. B* **102**, 245407 (2020).
- [35] F.-Q. Dou, Y.-Q. Lu, Y.-J. Wang, and J.-A. Sun, *Phys. Rev. B* **105**, 115405 (2022).
- [36] M. Hadipour, S. Haseli, D. Wang, and S. Haddadi, *Adv. Quantum Technol.* **7**, 2400115 (2024).
- [37] L. Wang, S.-Q. Liu, F.-L. Wu, H. Fan, and S.-Y. Liu, *Phys. Rev. A* **108**, 062402 (2023).
- [38] R. Grazi, D. Sacco Shaikh, M. Sasseti, N. Traverso Ziani, and D. Ferraro, *Phys. Rev. Lett.* **133**, 197001 (2024).
- [39] Y. Yao and X. Q. Shao, *Phys. Rev. E* **106**, 014138 (2022).
- [40] F. Zhao, F.-Q. Dou, and Q. Zhao, *Phys. Rev. A* **103**, 033715 (2021).
- [41] V. Evangelakos, E. Paspalakis, and D. Stefanatos, *Phys. Rev. A* **110**, 052601 (2024).
- [42] R. Salvia, M. Perarnau-Llobet, G. Haack, N. Brunner, and S. Nimmrichter, *Phys. Rev. Res.* **5**, 013155 (2023).
- [43] L. Peng, W. B. He, S. Chesi, H. Q. Lin, and X. W. Guan, *Phys. Rev. A* **103**, 052220 (2021).
- [44] H.-L. Shi, S. Ding, Q.-K. Wan, X.-H. Wang, and W.-L.

- Yang, *Phys. Rev. Lett.* **129**, 130602 (2022).
- [45] T. P. Le, J. Levinsen, K. Modi, M. M. Parish, and F. A. Pollock, *Phys. Rev. A* **97**, 022106 (2018).
- [46] F.-Q. Dou, Y.-J. Wang, and J.-A. Sun, (2022), [arXiv:2208.04831](https://arxiv.org/abs/2208.04831).
- [47] S. Ghosh and A. Sen(De), *Phys. Rev. A* **105**, 022628 (2022).
- [48] A. Ali, S. Al-Kuwari, M. I. Hussain, T. Byrnes, M. T. Rahim, J. Q. Quach, M. Ghominejad, and S. Haddadi, *Phys. Rev. A* **110**, 052404 (2024).
- [49] S. Ghosh, T. Chanda, and A. Sen(De), *Phys. Rev. A* **101**, 032115 (2020).
- [50] Y. Huangfu and J. Jing, *Phys. Rev. E* **104**, 024129 (2021).
- [51] D. Rossini, G. M. Andolina, and M. Polini, *Phys. Rev. B* **100**, 115142 (2019).
- [52] L. F. C. de Moraes, A. C. Duriez, A. Saguia, A. C. Santos, and M. S. Sarandy, *Quantum Sci. Technol.* **9**, 045033 (2024).
- [53] T. K. Konar, L. G. C. Lakkaraju, and A. Sen (De), *Phys. Rev. A* **109**, 042207 (2024).
- [54] F. H. Kamin, F. T. Tabesh, S. Salimi, and A. C. Santos, *Phys. Rev. E* **102**, 052109 (2020).
- [55] B. Mojaveri, R. Jafarzadeh Bahrbeig, and M. A. Fasihi, *Phys. Rev. A* **109**, 042619 (2024).
- [56] S.-Q. Liu, L. Wang, H. Fan, F.-L. Wu, and S.-Y. Liu, *Phys. Rev. A* **109**, 042411 (2024).
- [57] P. Chen, T. S. Yin, Z. Q. Jiang, and G. R. Jin, *Phys. Rev. E* **106**, 054119 (2022).
- [58] L. Gao, C. Cheng, W.-B. He, R. Mondaini, X.-W. Guan, and H.-Q. Lin, *Phys. Rev. Res.* **4**, 043150 (2022).
- [59] F.-Q. Dou, H. Zhou, and J.-A. Sun, *Phys. Rev. A* **106**, 032212 (2022).
- [60] K. Xu, H.-J. Zhu, G.-F. Zhang, and W.-M. Liu, *Phys. Rev. E* **104**, 064143 (2021).
- [61] D. Farina, G. M. Andolina, A. Mari, M. Polini, and V. Giovannetti, *Phys. Rev. B* **99**, 035421 (2019).
- [62] F.-M. Yang and F.-Q. Dou, *Phys. Rev. A* **109**, 062432 (2024).
- [63] F.-Q. Dou and F.-M. Yang, *Phys. Rev. A* **107**, 023725 (2023).
- [64] F. T. Tabesh, F. H. Kamin, and S. Salimi, *Phys. Rev. A* **102**, 052223 (2020).
- [65] F. Caravelli, B. Yan, L. P. García-Pintos, and A. Hama, *Quantum* **5**, 505 (2021).
- [66] S. Zakavati, F. T. Tabesh, and S. Salimi, *Phys. Rev. E* **104**, 054117 (2021).
- [67] D.-Y. Zhang, S.-Q. Ma, Y.-X. Jiang, Y.-B. Yu, G.-R. Jin, and A.-X. Chen, *Phys. Rev. A* **110**, 032211 (2024).
- [68] K. V. Hovhannisyann, M. Perarnau-Llobet, M. Huber, and A. Acín, *Phys. Rev. Lett.* **111**, 240401 (2013).
- [69] M. Gumberidze, M. Kolář, and R. Filip, *Sci. Rep.* **9**, 19628 (2019).
- [70] G. Zhu, Y. Chen, Y. Hasegawa, and P. Xue, *Phys. Rev. Lett.* **131**, 240401 (2023).
- [71] F.-Q. Dou, Y.-J. Wang, and J.-A. Sun, *Front. Phys.* **17**, 31503 (2021).
- [72] J.-Y. Gyhm, D. Šafránek, and D. Rosa, *Phys. Rev. Lett.* **128**, 140501 (2022).
- [73] Y.-Y. Zhang, T.-R. Yang, L. Fu, and X. Wang, *Phys. Rev. E* **99**, 052106 (2019).
- [74] C. A. Downing and M. S. Ukhtary, *Phys. Rev. A* **109**, 052206 (2024).
- [75] F. Mazzoncini, V. Cavina, G. M. Andolina, P. A. Erdman, and V. Giovannetti, *Phys. Rev. A* **107**, 032218 (2023).
- [76] R. R. Rodríguez, B. Ahmadi, G. Suárez, P. Mazurek, S. Barzanjeh, and P. Horodecki, *New J. Phys.* **26**, 043004 (2024).
- [77] A. Mitra and S. C. L. Srivastava, *Phys. Rev. A* **110**, 012227 (2024).
- [78] H.-Y. Yang, H.-L. Shi, Q.-K. Wan, K. Zhang, X.-H. Wang, and W.-L. Yang, *Phys. Rev. A* **109**, 012204 (2024).
- [79] W.-L. Song, H.-B. Liu, B. Zhou, W.-L. Yang, and J.-H. An, *Phys. Rev. Lett.* **132**, 090401 (2024).
- [80] K. Xu, H.-G. Li, H.-J. Zhu, and W.-M. Liu, *Phys. Rev. E* **109**, 054132 (2024).
- [81] G. Bhanja, D. Tiwari, and S. Banerjee, *Phys. Rev. A* **109**, 012224 (2024).
- [82] G. Carleo, I. Cirac, K. Cranmer, L. Daudet, M. Schuld, N. Tishby, L. Vogt-Maranto, and L. Zdeborová, *Rev. Mod. Phys.* **91**, 045002 (2019).
- [83] P. Zhang, H. Shen, and H. Zhai, *Phys. Rev. Lett.* **120**, 066401 (2018).
- [84] K. Kottmann, F. Metz, J. Fraxanet, and N. Baldelli, *Phys. Rev. Res.* **3**, 043184 (2021).
- [85] A. Jasinski, J. Montaner, R. C. Forrey, B. H. Yang, P. C. Stancil, N. Balakrishnan, J. Dai, R. A. Vargas-Hernández, and R. V. Krems, *Phys. Rev. Res.* **2**, 032051 (2020).
- [86] S. Jerbi, L. M. Trenkwalder, H. Poulsen Nautrup, H. J. Briegel, and V. Dunjko, *PRX Quantum* **2**, 010328 (2021).
- [87] T. Fösel, P. Tighineanu, T. Weiss, and F. Marquardt, *Phys. Rev. X* **8**, 031084 (2018).
- [88] S. Borah, B. Sarma, M. Kewming, G. J. Milburn, and J. Twamley, *Phys. Rev. Lett.* **127**, 190403 (2021).
- [89] Y.-H. Zhang, P.-L. Zheng, Y. Zhang, and D.-L. Deng, *Phys. Rev. Lett.* **125**, 170501 (2020).
- [90] A. Bolens and M. Heyl, *Phys. Rev. Lett.* **127**, 110502 (2021).
- [91] P. A. Erdman, G. M. Andolina, V. Giovannetti, and F. Noé, (2023), [arXiv:2212.12397](https://arxiv.org/abs/2212.12397).
- [92] C. Rodríguez, D. Rosa, and J. Olle, *Phys. Rev. A* **108**, 042618 (2023).
- [93] T. Haarnoja, A. Zhou, K. Hartikainen, G. Tucker, S. Ha, J. Tan, V. Kumar, H. Zhu, A. Gupta, P. Abbeel, and S. Levine, (2018), [arXiv:1812.05905](https://arxiv.org/abs/1812.05905).
- [94] T. Haarnoja, A. Zhou, P. Abbeel, and S. Levine, (2018), [arXiv:1801.01290](https://arxiv.org/abs/1801.01290).
- [95] A. Paszke, S. Gross, F. Massa, A. Lerer, J. Bradbury, G. Chanan, T. Killeen, Z. Lin, N. Gimelshein, L. Antiga, A. Desmaison, A. Köpf, E. Yang, Z. DeVito, M. Raison, A. Tejani, S. Chilamkurthy, B. Steiner, L. Fang, J. Bai, and S. Chintala, *Adv. Neural. Inf. Process. Syst.* **32**, 8026 (2019).
- [96] J. Johansson, P. Nation, and F. Nori, *Comput. Phys. Commun.* **184**, 1234 (2013).
- [97] M. B. Plenio, *Phys. Rev. Lett.* **95**, 090503 (2005).
- [98] P. A. Erdman and F. Noé, *npj Quantum Inf.* **8**, 1 (2022).
- [99] J. Q. Quach and W. J. Munro, *Phys. Rev. Appl.* **14**, 024092 (2020).